Journal of Materials Chemistry A

PAPER

View Article Online
View Journal | View Issue

Cite this: J. Mater. Chem. A, 2014, 2, 4406

Polybenzoxazine-based monodisperse carbon spheres with low-thermal shrinkage and their CO_2 adsorption properties†

Shuai Wang, Wen-Cui Li, Ling Zhang, Zhen-Yu Jin and An-Hui Lu*

Received 6th December 2013
Accepted 6th January 2014

DOI: 10.1039/c3ta15065h

www.rsc.org/MaterialsA

We describe the synthesis of polybenzoxazine-based spheres that can be carbonized with little shrinkage to produce monodisperse carbon spheres with abundant porosity. The porous structure of the carbon spheres was analyzed by nitrogen sorption isotherms. Elemental analysis, infrared spectroscopy and $^{1}H \rightarrow {}^{13}C$ CP/MAS NMR analysis were carried to characterize the surface chemistry of the spheres. The porous carbon spheres contain intrinsic nitrogen-containing groups that make them more useful for CO_2 adsorption. The CO_2 adsorption capacity can reach 11.03 mmol g^{-1} (*i.e.* 485 mg g^{-1}) at −50 °C and ~1 bar, which is highly desirable for the CO_2 separation from natural gas feeds during the cryogenic process to produce liquefied natural gas. Moreover, the prepared carbon spheres show the highest adsorption capacity for CO_2 per cm^3 micropore volume, when compared with recently reported carbon adsorbents with high CO_2 capture capacities at low temperature. Due to the uniform size and low thermal shrinkage during production, the carbon spheres were also used as models to investigate the influence of porous structure and surface chemistry on CO_2 adsorption behavior. The porosity plays an essential role in achieving high CO_2 adsorption capacity at ambient pressure, while the nitrogen content of the carbon adsorbent is a booster for CO_2 adsorption capacity at low pressures. This finding may be beneficial to design sorbents for the separation of dilute CO_2-containing gas streams in practical applications.

1 Introduction

Porous carbons can have a number of advantageous properties, such as high surface area, good chemical stability and electrical conductivity, that enable them to be widely used in adsorption,[1–5] energy storage,[6–10] catalysis[11–14] and drug delivery.[15–18] Nanoporous carbon spheres have long been attractive because of their high surface-to-volume ratio, good structural stability, and void space for encapsulating large quantities of guest molecules.[19–21] All of these features make them especially suitable in the fields of gas adsorption and separation. Up to now, the favored method for the synthesis of uniform spherical carbons relies on the carbonization of pre-synthesized polymer spheres.[22–24] Traditionally, the polymer spheres undergo an obvious shrinkage during carbonization at 500–900 °C.[25] Although some polymer spheres (polypyrrole nanospheres, for example) have a low shrinkage during carbonization, they usually do not exhibit any open porosity.[6,7,26] Recently, we have described a new polymerization system to synthesize polybenzoxazine-based carbon spheres.[27] The carbonization involves low shrinkage and produces abundant porosity. Importantly, such carbon spheres contain intrinsic nitrogen-containing groups that make them more useful for carbon dioxide adsorption.[28–31]

Carbon dioxide (CO_2) is widely regarded as one of the main greenhouse gases. It is also highly detrimental in some special gas streams. For example, natural gas from wells often contains fairly high amounts of CO_2, which significantly reduces its energy content. Natural gas is a clean and efficient energy resource and liquefied natural gas (LNG) can be easily transported and stored due to its high energy density. Although producing one ton of LNG consumes about 850 kWh of electric energy,[32] 28.2 percent of the international natural gas trade was in the form of LNG in 2006.[33]

Generally, LNG is produced by cryogenic refrigeration of natural gas in which the first step is to remove water and CO_2 at atmospheric pressure and a temperature of approximately −162 °C. The formation of frozen solid CO_2 separated from the feed gas has a destructive effect on equipment and efficiency during the liquefaction process.[34,35] Moreover, the separation of CO_2 from feed gases with a carbon dioxide concentration

State Key Laboratory of Fine Chemicals, School of Chemical Engineering, Dalian University of Technology, Dalian 116024, P. R. China. E-mail: anhuilu@dlut.edu.cn; Fax: +86 411 84986112; Tel: +86 411 84986112

† Electronic supplementary information (ESI) available: Cumulative volume of CBD-800 and CBDC-900 at different pore sizes. Comparison of the prepared carbon spheres and recently reported microporous carbon adsorbents for CO_2 capture at ~1 bar and 25, 0 or −50 °C. CO_2 adsorption isotherms and CH_4 sorption isotherm of CBDC-900 measured at −50 °C. CO_2 adsorption isotherms of CBD-800 measured at 0 °C. See DOI: 10.1039/c3ta15065h

between 0.1 and 15 v% continues to be a problem during the cryogenic handling procedure. Great efforts have therefore been directed towards the development of new technologies and materials for CO_2 adsorption and separation.[36–40] Among these approaches, adsorption on porous solids is considered to be one of the most competitive approaches because of its low cost, easy application and good cycle performance.[1,30,41–45]

It is well known that the CO_2 adsorption capacity increases with a decrease of the adsorption temperature. In order to have a more efficient use of the energy used for liquefaction and achieve an effective adsorption of CO_2, it is necessary to find a CO_2 adsorption material which shows a high adsorption capacity at a low temperature before the CO_2 solidifies. Here, we report the development of polybenzoxazine-based carbon spheres that involve a low shrinkage during carbonization. The prepared N-doped carbon spheres show a CO_2 uptake of 11.03 mmol g^{-1} (*i.e.* 485 mg g^{-1}) at −50 °C and 1 atm, with the highest adsorption capacity for CO_2 per cm^3 micropore volume. The high CO_2 adsorption capacity at low temperature makes them suitable for gas purification.[46] Due to their uniform size and low thermal shrinkage during carbonization, they can also be used as models to investigate the influence of pore structure and surface chemistry on CO_2 adsorption.

2 Experimental section

2.1 Materials

Resorcinol (99.5%), and formaldehyde (37 wt%), were purchased from Tianjin Kermel Chemical Reagent Co., Ltd. 1,6-Diaminohexane (DAH, 99.0%) was supplied by Sinopharm Chemical Reagent Co., Ltd. Pluronic F127 was purchased from Fluka. All chemicals were used as received.

2.2 Preparation of monodisperse polymer and carbon spheres

Typically, 1 mmol resorcinol was first dissolved in 200 g deionized water with vigorous stirring at an initial reaction temperature of 24 °C, and then 0.004 mmol F127 and 2 mmol formaldehyde (37 wt%) were added to form a clear solution. After the addition of a certain amount of DAH, the clear solution became a white colloid within a minute. The resultant solution was further heated to 80 °C for 18 h accompanied by vigorous stirring. The polymers obtained were washed three times with distilled water with each wash followed by centrifugation to separate the polymer from other soluble components. The following molar ratios of resorcinol and DAH were used 1 : 0.125, 1 : 0.25, 1 : 0.50 to 1 : 0.75 and the obtained polymers were accordingly denoted PBD-1, PBD-2, PBD-3 and PBD-4. Carbon spheres were obtained by pyrolysis of PBD-2 at 500 °C, 600 °C, 700 °C and 800 °C for 2 h under a nitrogen atmosphere, and the obtained carbon spheres were accordingly denoted CBD-500, CBD-600, CBD-700 and CBD-800. The sample CBDC-900 was obtained by pyrolysis of PBD-2 at 800 °C for 2 h under a nitrogen atmosphere, and then activated at 900 °C for 1 h in CO_2.

2.3 Characterization method

Scanning electron microscopy (SEM) investigations were carried out with a Hitachi S-4800 instrument. The NMR experiments were performed on a Varian Infinity-plus 400 spectrometer operating at a magnetic field strength of 9.4 T. The resonance frequency at this field strength was 100.5 MHz for ^{13}C. A Chemagnetics 4 mm double-resonance MAS probe was used to acquire all the spectra with a spinning rate of 6 kHz. The variable amplitude cross polarization (VACP) technique was used in the $^{1}H \rightarrow {}^{13}C$ CP/MAS experiment. Radio fields of 80 kHz were used on ^{1}H nuclei, and a linear ramp of 1 kHz centered around 86 kHz was used on ^{13}C nuclei at the −1 Hartman–Hahn sideband condition. The contact time for cross polarization was 5 ms and the recycle delay was 2 s. The ^{13}C chemical shift was referenced to hexamethylbenzene (HMB). Before the CP/MAS NMR measurements, the sample was ground into a fine powder. Elemental analysis was carried out on a CHNO elemental analyzer (Vario EL III, Elementar). The IR spectrum was collected on a Nicolet 6700 FTIR spectrometer. X-ray photoelectron spectroscopy (XPS) measurements were performed using a Thermo VG Scientific ESCALAB 250Xi spectrometer with Al Kα radiation (1486.6 eV).

CO_2, CH_4 and N_2 adsorption isotherms were measured with a Micromeritics ASAP 2020 adsorption analyzer. Prior to each adsorption experiment, the sample was degassed for 6 h at 200 °C, ensuring that the residual pressure fell below 5×10^{-3} mbar, and then cooled to the target temperature, followed by the introduction of a single component gas (CO_2, CH_4 or N_2) into the system. The Brunauer–Emmett–Teller (BET) method was used to calculate the specific surface area. Total pore volumes (V_{total}) were calculated from the amount of nitrogen adsorbed at a relative pressure, P/P_0, of 0.95. The pore size distribution and the cumulative volume were determined from the N_2 adsorption branches of the isotherm using the Density Functional Theory (DFT) method.

3 Results and discussion

Because the functional groups and the polymerization rate of the polybenzoxazine systems can be influenced by the amount of 1,6-diaminohexane (DAH) used in the synthesis, in this study we first investigated the effects caused by the of the amount of DAH used. As shown by the SEM observations (Fig. 1a and b), one can see that the products obtained with the use of a molar ratio of resorcinol to DAH of 1 : 0.125 (PBD-1) and 1 : 0.25 (PBD-2) show a perfectly spherical morphology and uniformity in particle sizes (188 ± 5 nm and 184 ± 6 nm, respectively). Moreover, self-assembled periodic structures with close-packed planes arranged along the (111) direction are observed,[47] indicating that the polymer spheres are monodispersed.[48] When the molar ratio of resorcinol to DAH is 1 : 0.50, the obtained sample (PBD-3) shows an average particle size of 219 ± 5 nm, accompanied by some nonspherical dimer and trimer colloidal particles (Fig. 1c). When using the molar ratio of 1 : 0.75, the synthesized polymer product PBD-4 exhibits a continuous framework composed of crosslinked spherical colloidal

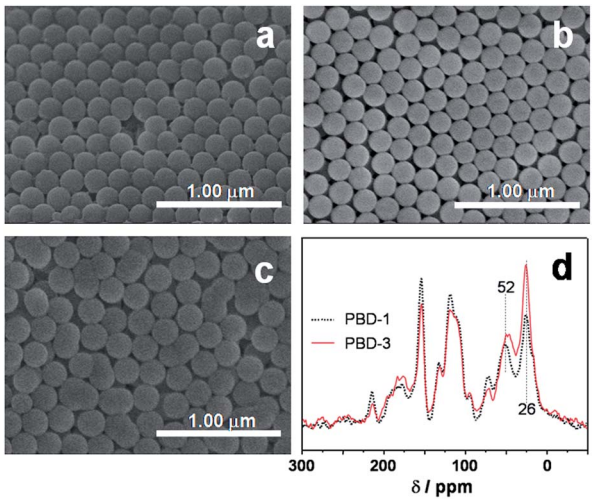

Fig. 1 SEM images of the polymer spheres (a) PBD-1, (b) PBD-2 and (c) PBD-3 prepared at different molar ratios of resorcinol to DAH. (d) $^{1}H \rightarrow {}^{13}C$ CP/MAS NMR spectra of PBD-1 and PBD-3.

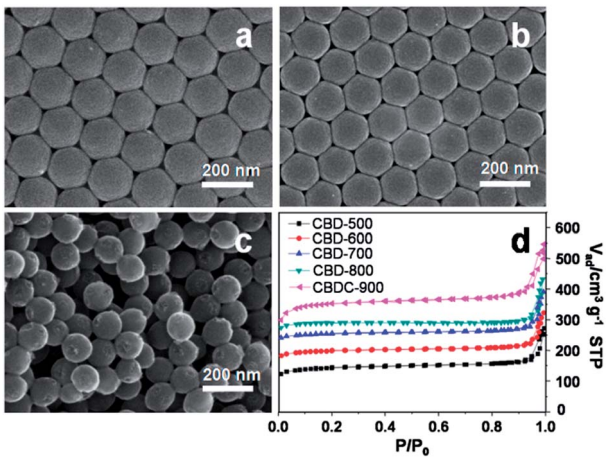

Fig. 2 SEM images of the carbon spheres (a) CBD-500, (b) CBD-800 and (c) CBDC-900. (d) Nitrogen sorption isotherms of carbon spheres produced by carbonization under different conditions. The nitrogen sorption isotherms of CBD-600, CBD-700 and CBD-800 are vertically offset by 50, 100, 100 $cm^3\ g^{-1}$, STP.

particles (not shown here). One possible explanation is that the DAH molecules on the sphere surface induce polymerization between the colloidal particles and further aggregation of particles.

To further demonstrate the role of DAH, $^{1}H \rightarrow {}^{13}C$ CP/MAS NMR analyses were carried out. As shown in Fig. 1d, the strong and broad signals with chemical shifts ranging from 100 to 175 ppm are attributed to the carbons in the aromatic rings of the resorcinol–formaldehyde polymer networks. The $^{1}H \rightarrow {}^{13}C$ CP/MAS NMR spectra of the as-made polymer shows resolved peaks at ~53 and ~26 ppm, derived from a Mannich reaction, which can be attributed to the methylene groups in Ar-CH_2–N– and –$(CH_2)_6$– respectively. As the amount of DAH used is increased (sample PBD-3), the intensities of the peaks at ~53 and ~26 ppm gradually increase, indicating that more DAH participates in the polymerization to form polybenzoxazines.[49] The further polymerization not only leads to an increase in the crosslinking degree inside the polymer particles but also initiates more opportunities for the surface crosslinking of individual polymer spheres. It thus results in particle aggregation, as shown by the SEM image in Fig. 1c.

It is clear that the polymer spheres with a higher degree of crosslinking show better thermal stability under carbonization conditions. And when the polymer spheres are subjected to carbonization, the characteristic parameter of the carbonized derivatives highly depends on the carbonization conditions. We therefore chose PBD-2, which has a perfectly spherical shape with a high degree of crosslinking, as a representative carbon precursor to undergo thermal treatment at temperatures from 500 °C to 800 °C under a nitrogen atmosphere. The obtained carbon samples were accordingly denoted CBD-500, CBD-600, CBD-700 and CBD-800.

As shown in Fig. 2a and b the carbon products retain a perfectly spherical shape and are highly uniform in size, indicating the good thermal and shape stability of the polymer spheres. The particle sizes of PBD-2 change from 184 ± 6 to 155 ± 4 nm after the thermal treatment at 500 °C, and the particle sizes change to 139 ± 4 nm after further carbonization at 800 °C. Between 500 and 800 °C, the sphere sizes show a linear shrinkage of only 10.3%, indicating good thermal stability. Although the particle sizes of such spheres do not show an obvious change upon carbonization, their pore structures and nitrogen contents depend on the carbonization conditions.[50]

The porosity of the carbon spheres was analyzed using nitrogen sorption at −196 °C. The nitrogen sorption isotherms are of Type I (Fig. 2d), indicating the materials are microporous. The sharp nitrogen uptake of the isotherms in the relative pressure range of 0.9–1.0 is attributed to nitrogen molecule condensation in the nanospaces between the close-packed carbon spheres, which can also be seen in Fig. 2a and b. As shown in Table 1, we can see that carbonization at an elevated temperature leads to a developed porosity, and the BET surface area and the micropore volume increase with carbonization temperature. The chemical compositions of the polymer and carbon samples are also shown in Table 1. It can be seen that all samples contain nitrogen due to the intrinsic nitrogen content of the polybenzoxazine spheres. The nitrogen content in the carbon samples decreased as the carbonization temperature increased.

FT-IR analysis (Fig. 3) was also used to confirm the existence of basic functional groups. The band at around 3450 cm^{-1} may be related to N–H or O–H stretching vibrations or water molecules. The peaks around 1600 cm^{-1} and 1250 cm^{-1} are attributed to N–H in-plane deformation vibrations and the C–N stretching vibration, respectively. The broad medium-strong bands between 950 and 650 cm^{-1} correspond to the out-of-plane N–H deformation vibration. Hence, the as-made carbon materials inherently have developed pore structures and nitrogen-containing groups.

Table 1 Physical properties and elemental analysis of the polymer and carbon spheres

	Physical properties[a]			Elemental analysis		
Sample	S_{BET}/m^2 g^{-1}	V_{total}/cm^3 g^{-1}	V_{micro}/cm^3 g^{-1}	N/wt%	C/wt%	H/wt%
PBD-2	—	—	—	3.71	62.63	6.34
CBD-500	484	0.26	0.18	2.20	75.56	6.34
CBD-600	501	0.27	0.19	2.26	82.36	2.12
CBD-700	520	0.28	0.21	1.74	89.06	1.04
CBD-800	635	0.32	0.27	1.52	90.61	0.68
CBDC-900	1188	0.63	0.46	1.74	86.74	1.02

[a] S_{BET}: the surface area calculated by the Brunauer–Emmett–Teller (BET) method, V_{micro}: micropore volume calculated by a *t*-plot analysis, V_{total}: total pore volume at $P/P_0 = 0.95$.

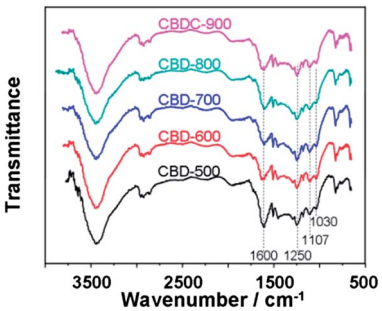

Fig. 3 FT-IR spectra of carbon spheres produced by carbonization at different temperatures.

N-doped porous carbon is generally considered to be one of the most promising candidates for CO_2 adsorption.[51,52] Hence, the microporous N-doped carbon spheres were used as models to study the adsorption behavior of CO_2. The CO_2 adsorption performance of all samples was examined using a Micromeritics ASAP 2020 static volumetric analyzer at 25 °C, and for comparison, also measured at 0 °C. The obtained carbon spheres show elbow-shaped CO_2 adsorption isotherms in the ambient pressure region. Their high permeability facilitates the diffusion of CO_2 molecules, and Lewis base active sites of nitrogen-containing groups increase the binding of CO_2.[53] Thus, the carbon spheres exhibit a high CO_2 uptake. Moreover, the nitrogen-doped carbon spheres show high CO_2 uptake at a low pressure (~150 mmHg) (Fig. 4). This CO_2 adsorption capacity is comparable to or even higher than that of most MOF materials under identical adsorption conditions.[54,55]

As shown in Fig. 4a and b, the CO_2 adsorption capacities increase with the porosity of the carbon spheres as the carbonization temperatures increase from 500 °C to 800 °C. The structure parameters of the carbon spheres seems to have an important influence on the adsorption capacity of CO_2,[56] as the CBD-500 prepared at the lowest carbonization temperature of 500 °C shows the lowest CO_2 adsorption capacity at 25 °C and 0 °C. CBD-800 with a developed porous structure has a higher adsorption capacity of 4.36 mmol g^{-1} at 0 °C and ~1 bar (3.21 mmol g^{-1} at 25 °C). To further improve micropore volume, CBD-800 was activated at 900 °C for 1 h under CO_2 (the sample obtained was denoted CBDC-900).[57] Sample CBDC-900 consists of uniform spheres with a diameter of 105 ± 3 nm (Fig. 2c), and has the highest BET surface area and micropore volume (Table 1) of all the samples. CO_2 adsorption is not limited by the total pore volume but only by pores smaller than a certain diameter.[58] The cumulative volume of CBDC-900 at different pore size is larger than that of CBD-800 (Table S1†), indicating that activation not only has widened the existing micropores but also has created more narrow micropores. Its CO_2 adsorption capacity also increases to 5.16 mmol g^{-1} at 0 °C and ~1 bar (3.39 mmol g^{-1} at 25 °C). This means that the developed porous structure plays a significant role at ambient pressure for achieving high CO_2 adsorption capacity.[59–61]

In order to separate CO_2 from the natural gas feed and use the cryogenic energy of producing LNG, as a case study, samples CBD-800 and CBDC-900 with a high CO_2 adsorption capacity at 25 °C and 0 °C were further tested at −50 °C. The better porosity developed in CBDC-900 also shows a higher CO_2 adsorption capacity of 11.03 mmol g^{-1} (*i.e.* 485 mg g^{-1}) than that of CBD-800 (7.84 mmol g^{-1}, *i.e.* 345 mg g^{-1}) at −50 °C and ~1 bar

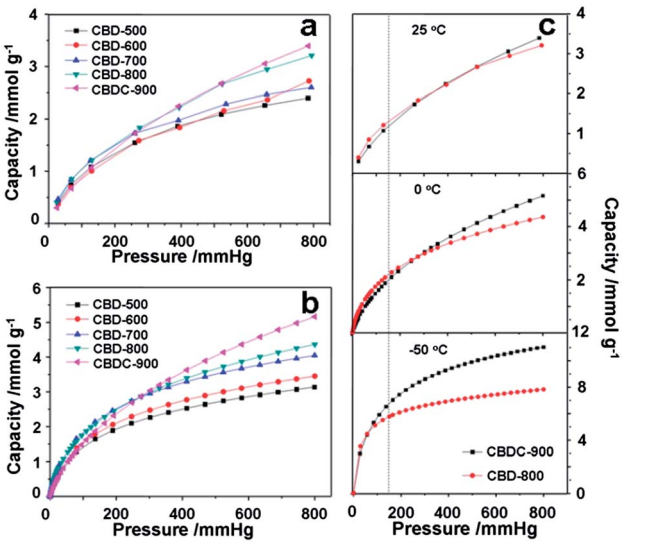

Fig. 4 CO_2-adsorption isotherms of the carbon samples at (a) 25 °C, (b) 0 °C at ambient pressure. (c) The CO_2-adsorption isotherms of CBD-800 and CBDC-900 at 25 °C, 0 °C and −50 °C were also compiled for clarity.

(Fig. 4c). And the adsorption capacities of CBDC-900 for CH_4 are much lower as compared to those for CO_2 under the same pressure, with a maximum of 3.42 mmol g^{-1} at ambient pressure at −50 °C (Fig. S1†). The high CO_2 adsorption capacity and good selectivity at low temperature makes the carbon spheres suitable for the separation of CO_2 in the process of producing LNG. Moreover, the adsorption capacities for CO_2 per cm^3 micropore volume of CBD-800 and CBDC-900 were also compared with recently reported adsorbents with high CO_2 capture capacities (Fig. 5, Table S2†). At 1 bar and 0 °C, based on the micropore volume, CBD-800 shows CO_2 adsorption capacity of 16.1 mol cm^{-3}, indicating the highest utilization degree of micropores compared to the above mentioned porous carbons. The recyclability of CO_2 adsorption on CBD-800 has been tested for 4 cycles at 0 °C. As seen in Fig. S2,† the sample shows almost constant CO_2 adsorption capacities under the same conditions during cycling. This indicates that the carbon spheres retain good stability for CO_2 capture.

With lower total pressure, pores smaller or equal to 0.5 nm are preferred CO_2 adsorption.[58] Compared with CBD-800, the sample CBDC-900 has a greater contribution of narrow micropores smaller or equal to 0.5 nm (Table S1,† Fig. 6a). However CBDC-900 shows a lower CO_2 adsorption capacity than CBD-800 in the low pressure range at 0 °C and 25 °C (Fig. 4c). This may be due to the high surface area of CBDC-900 causing a high dilution of nitrogen-containing groups.[62] Moreover, CBDC-900 shows a lower surface content of nitrogen (0.9 wt%) than CBD-800 (1.6 wt%), detected by XPS, which weakens the interaction of the CO_2 molecules with the N-doped carbon. To determine the strength of the interaction between CO_2 molecules and the carbon materials at low pressures, the isosteric heat of adsorption (Q_{st}) for CBD-800 and CBDC-900 were calculated using the CO_2 sorption isotherms measured at 223, 273 and 298 K based on the Clausius–Clapeyron equation. As shown in Fig. 6b, the initial Q_{st} for CBD-800 is in the range of 35–37 kJ mol^{-1} at low CO_2 adsorption, while CBDC-900 with greater porosity shows a lower initial Q_{st} of 22 kJ mol^{-1}. This indicates a stronger interaction between the CO_2 molecules and the N-doped carbon pore walls of CBD-800 in low surface coverage at ~0.1 bar.[28]

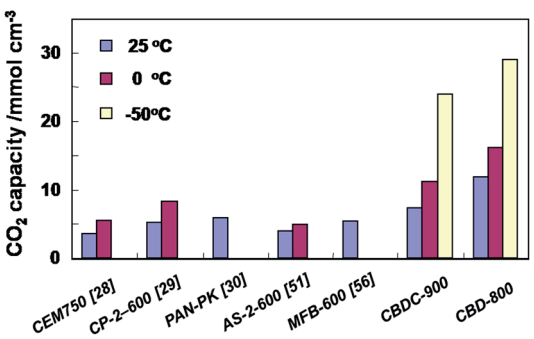

Fig. 5 The comparison of adsorption capacities for CO_2 per cm^3 micropore volume of CBD-800 and CBDC-900 from the present work with several recently reported porous carbon adsorbents. The CO_2 adsorption capacities were collected at 1 bar and 25 °C, 0 °C, −50 °C.

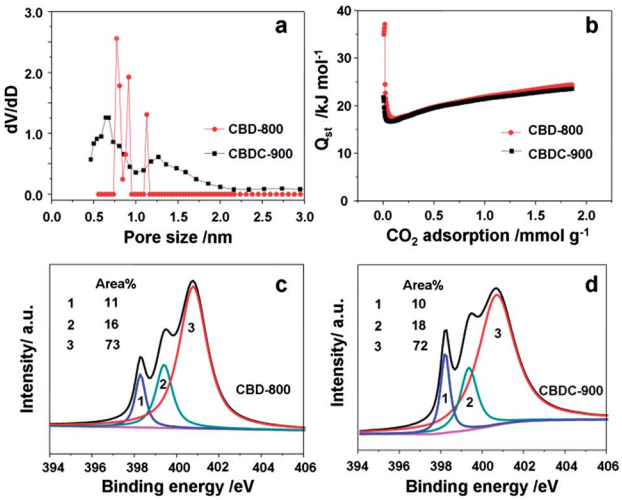

Fig. 6 Pore size distribution (a) and isosteric heat of CO_2 adsorption (b) for CBD-800 and CBDC-900. XPS N 1s narrow-scan spectra of CBD-800 (c) and CBDC-900 (d).

The nature of the nitrogen species on the surface of CBD-800 and CBDC-900 was further investigated by XPS (Fig. 6c and d). Three different types of nitrogen species can be distinguished on both sample surfaces, *i.e.* pyridinic-N (398.7 ± 0.3 eV), pyrrolic-N or pyridonic-N nitrogen (400.3 ± 0.3 eV) and quaternary nitrogen (401.4 ± 0.5 eV).[29,52] Pyridonic-N[29] or pyrrolic-N[31] could interact with CO_2 by N–H···O hydrogen bonding and by an interaction between the N lone pair electrons and the C atom of CO_2 for coverage at low pressure.[63,64] The reduced thermal motion of CO_2 molecules causes them to interact with the nitrogen-containing groups less as temperature decreases to −50 °C, and the contribution of nitrogen-containing groups for the adsorption capability can be weakened. CBDC-900 shows higher CO_2 uptakes as the pressure increases (Fig. 4c). Compared with the other adsorbents in Fig. 4a and b, we can see that, in the adsorption process, the porous structure plays a dominant role as the CO_2 pressure reaches atmospheric pressure, while a higher nitrogen content is beneficial to improve CO_2 adsorption capacity at a low partial pressure, especially for the materials with poor porosity. This is an important point which can be taken into account when designing sorbents for dilute CO_2 adsorption and separation in practical applications.

4 Conclusions

In this study, we have produced novel polybenzoxazine-based carbon spheres that have a uniform size, and undergo a low shrinkage during carbonization, and investigated their CO_2 adsorption properties. The CO_2 adsorption capacity can reach 11.03 mmol g^{-1} (*i.e.* 485 mg g^{-1}) at −50 °C under and ~1 bar, which is a very high value, indicating this type of carbon spheres is highly desirable for the separation of CO_2 from natural gas feeds, when a cryogenic process is used to produce liquefied

natural gas. More importantly, we find the nitrogen content and porosity play different roles in the CO_2 adsorption process. The nitrogen content of an adsorbent is a booster for CO_2 adsorption capacity at low pressures, while the porosity plays an essential role in achieving high CO_2 adsorption capacity at ambient pressure. This study may provide a new aspect for the design of sorbents for the separation of dilute CO_2-containing gas streams in practical applications.

Acknowledgements

The project was supported by the Special Program for Basic Research of the Ministry of Science and Technology (2012CB626802) and NSFC (no. 21073026).

Notes and references

1 G. P. Hao, W. C. Li and A. H. Lu, *J. Mater. Chem.*, 2011, **21**, 6447.
2 L. M. Guo, J. M. Zhang, Q. J. He, L. X. Zhang, J. J. Zhao, Z. Y. Zhu, W. Wu, J. Zhang and J. L. Shi, *Chem. Commun.*, 2010, **46**, 7127.
3 Q. Ji, S. B. Yoon, J. P. Hill, A. Vinu, J. S. Yu and K. Ariga, *J. Am. Chem. Soc.*, 2009, **131**, 4220.
4 H. Wang, Q. Gao and J. Hu, *J. Am. Chem. Soc.*, 2009, **131**, 7016.
5 Y. Xia, G. S. Walker, D. M. Grant and R. Mokaya, *J. Am. Chem. Soc.*, 2009, **131**, 16493.
6 F. Su, C. K. Poh, J. S. Chen, G. Xu, D. Wang, Q. Li, J. Lin and X. W. Lou, *Energy Environ. Sci.*, 2011, **4**, 717.
7 Y. Wang, F. Su, C. D. Wood, J. Y. Lee and X. S. Zhao, *Ind. Eng. Chem. Res.*, 2008, **47**, 2294.
8 X. Y. Chen, C. Chen, Z. J. Zhang, D. H. Xie, X. Deng and J. W. Liu, *J. Power Sources*, 2013, **230**, 50.
9 D. Li, F. Han, S. Wang, F. Cheng, Q. Sun and W. C. Li, *ACS Appl. Mater. Interfaces*, 2013, **5**, 2208.
10 Y. Fang, Y. Lv, R. Che, H. Wu, X. Zhang, D. Gu, G. Zheng and D. Zhao, *J. Am. Chem. Soc.*, 2013, **135**, 1524.
11 P. Serp, R. Feurer, Y. Kihn, P. Kalck, J. L. Fariad and J. L. Figueiredo, *J. Mater. Chem.*, 2001, **11**, 1980.
12 M. Gurrath, T. Kuretzky, H. P. Boehm, L. B. Okhlopkova, A. S. Lisitsyn and V. A. Likholobov, *Carbon*, 2000, **38**, 1241.
13 J. Y. Miao, D. W. Hwang, K. V. Narasimhulu, P. I. Lin, Y. T. Chen, S. H. Lin and L. P. Hwang, *Carbon*, 2004, **42**, 813.
14 Y. Önal, S. Schimpf and P. Claus, *J. Catal.*, 2004, **223**, 122.
15 Y. Fang, D. Gu, Y. Zou, Z. X. Wu, F. Y. Li, R. C. Che, Y. H. Deng, B. Tu and D. Y. Zhao, *Angew. Chem., Int. Ed.*, 2010, **49**, 7987.
16 M. Sevilla, P. Valle-Vigón, P. Tartaj and A. B. Fuertes, *Carbon*, 2009, **47**, 2519.
17 J. L. Gu, S. S. Su, Y. S. Li, Q. J. He and J. L. Shi, *Chem. Commun.*, 2011, **47**, 2101.
18 K. Ariga, A. Vinu, Y. Yamauchi, Q. Ji and J. P. Hill, *Bull. Chem. Soc. Jpn.*, 2012, **85**, 1.
19 S. H. Wu, C. Y. Mou and H. P. Lin, *Chem. Soc. Rev.*, 2013, **42**, 3862.
20 J. Yao, H. Wang, J. Liu, K. Y. Chan, L. Zhang and N. Xu, *Carbon*, 2005, **43**, 1709.
21 Z. Chen, C. Wang, J. Chen and X. Li, *J. Am. Chem. Soc.*, 2013, **135**, 4179.
22 Y. R. Dong, N. Nishiyama, Y. Egashira and K. Ueyama, *Ind. Eng. Chem. Res.*, 2008, **47**, 4712.
23 Y. Pan, M. Ju, C. Wang, L. Zhang and N. Xu, *Chem. Commun.*, 2010, **46**, 3732.
24 J. Liu, S. Z. Qiao, H. Liu, J. Chen, A. Orpe, D. Y. Zhao and G. H. Lu, *Angew. Chem., Int. Ed.*, 2011, **50**, 5947.
25 B. Friedel and S. Greulich-Weber, *Small*, 2006, **2**, 859.
26 F. B. Su, Z. Q. Tian, C. K. Poh, Z. Wang, S. H. Lim, Z. Liu and J. Lin, *Chem. Mater.*, 2010, **22**, 832.
27 S. Wang, W. C. Li, G. P. Hao, Y. Hao, Q. Sun, X. Q. Zhang and A. H. Lu, *J. Am. Chem. Soc.*, 2011, **133**, 15304.
28 Y. Xia, R. Mokaya, G. S. Walker and Y. Zhu, *Adv. Energy Mater.*, 2011, **1**, 678.
29 M. Sevilla, P. Valle-Vigón and A. B. Fuertes, *Adv. Funct. Mater.*, 2011, **21**, 2781.
30 W. Shen, S. Zhang, Y. He, J. Li and W. Fan, *J. Mater. Chem.*, 2011, **21**, 14036.
31 G. P. Hao, W. C. Li, D. Qian and A. H. Lu, *Adv. Mater.*, 2010, **22**, 853.
32 X. J. Shi and D. F. Che, *Energy Convers. Manage.*, 2009, **50**, 567.
33 C. Wen, X. Cao, Y. Yang, W. Li, W. S. Lin, N. Zhang and A. Z. Gu, *Energy*, 2010, **35**, 4383.
34 M. J. Tuinier, M. S. Annaland, G. J. Kramer and J. A. M. Kuipers, *Chem. Eng. Sci.*, 2010, **65**, 114.
35 G. Xu, L. Li, Y. P. Yang, L. H. Tian, T. Liu and K. Zhang, *Energy*, 2012, **42**, 522.
36 D. Qian, C. Lei, G. P. Hao, W. C. Li and A. H. Lu, *ACS Appl. Mater. Interfaces*, 2012, **4**, 6125.
37 D. M. D'Alessandro, B. Smit and J. R. Long, *Angew. Chem., Int. Ed.*, 2010, **49**, 6058.
38 F. M. Orr, Jr., *Energy Environ. Sci.*, 2009, **2**, 449.
39 K. M. K. Yu, I. Curcic, J. Gabriel and S. C. E. Tsang, *ChemSusChem*, 2008, **1**, 893.
40 S. Choi, J. H. Drese and C. W. Jones, *ChemSusChem*, 2009, **2**, 796.
41 Q. Wang, J. Luo, Z. Zhong and A. Borgna, *Energy Environ. Sci.*, 2011, **4**, 42.
42 J. Yu and B. Cheng, *RSC Adv.*, 2012, **2**, 6784.
43 L. B. Sun, J. Yang, J. H. Kou, F. N. Gu, Y. Chun, Y. Wang, J. H. Zhu and Z. G. Zou, *Angew. Chem., Int. Ed.*, 2008, **47**, 3418.
44 W. Cai, J. Yu, C. Anand, A. Vinu and M. Jaroniec, *Chem. Mater.*, 2011, **23**, 1147.
45 Y. Zhao, X. Liu, K. X. Yao, L. Zhao and Y. Han, *Chem. Mater.*, 2012, **24**, 4725.
46 Y. Belmabkhout, R. Serna-Guerrero and A. Sayari, *Ind. Eng. Chem. Res.*, 2010, **49**, 359.
47 M. Agrawal, D. Fischer, S. Gupta, N. E. Zafeiropoulos, A. Pich, E. Lidorikis and M. Stamm, *J. Phys. Chem. C*, 2010, **114**, 16389.
48 P. Jiang, J. F. Bertone and V. L. Colvin, *Science*, 2001, **291**, 453.

49 G. P. Hao, W. C. Li, D. Qian, G. H. Wang, W. P. Zhang, T. Zhang, A. Q. Wang, F. Schüth, H. J. Bongard and A. H. Lu, *J. Am. Chem. Soc.*, 2011, **133**, 11378.
50 M. Pérez-Cadenas, C. Moreno-Castilla, F. Carrasco-Marín and A. F. Pérez-Cadenas, *Langmuir*, 2009, **25**, 466.
51 M. Sevilla and A. B. Fuertes, *Energy Environ. Sci.*, 2011, **4**, 1765.
52 M. C. Gutiérrez, D. Carriazo, C. O. Ania, J. B. Parra, M. L. Ferrer and F. Del Monte, *Energy Environ. Sci.*, 2011, **4**, 3535.
53 M. D. Soutullo, C. I. Odom, B. F. Wicker, C. N. Henderson, A. C. Stenson and J. H. Davis, *Chem. Mater.*, 2007, **19**, 3581.
54 S. Ma and H. C. Zhou, *Chem. Commun.*, 2010, **46**, 44.
55 A. R. Millward and O. M. Yaghi, *J. Am. Chem. Soc.*, 2005, **127**, 17998.
56 C. Pevida, T. C. Drage and C. E. Snape, *Carbon*, 2008, **46**, 1464.
57 M. Molina-Sabio, M. T. Gonzalez, F. Rodriguez-Reinoso and A. Sepúlveda-Escribano, *Carbon*, 1996, **34**, 505.
58 V. Presser, J. McDonough, S. H. Yeon and Y. Gogotsi, *Energy Environ. Sci.*, 2011, **4**, 3059.
59 A. Wahby, J. M. Ramos-Fernández, M. Martínez-Escandell, A. Sepúlveda-Escribano, J. Silvestre-Albero and F. Rodríguez-Reinoso, *ChemSusChem*, 2010, **3**, 974.
60 Y. Zhang, B. Li, K. Williams, W. Y. Gao and S. Ma, *Chem. Commun.*, 2013, **49**, 10269.
61 Y. Li, T. Ben, B. Zhang, Y. Fu and S. Qiu, *Sci. Rep.*, 2013, **3**, 2420.
62 Y. Zhao, L. Zhao, K. X. Yao, Y. Yang, Q. Zhang and Y. Han, *J. Mater. Chem.*, 2012, **22**, 19726.
63 R. Vaidhyanathan, S. S. Iremonger, G. K. H. Shimizu, P. G. Boyd, S. Alavi and T. K. Woo, *Science*, 2010, **330**, 650.
64 R. Vaidhyanathan, S. S. Iremonger, K. W. Dawson and G. K. H. Shimizu, *Chem. Commun.*, 2009, 5230.

